Nanoscale

Accepted Manuscript

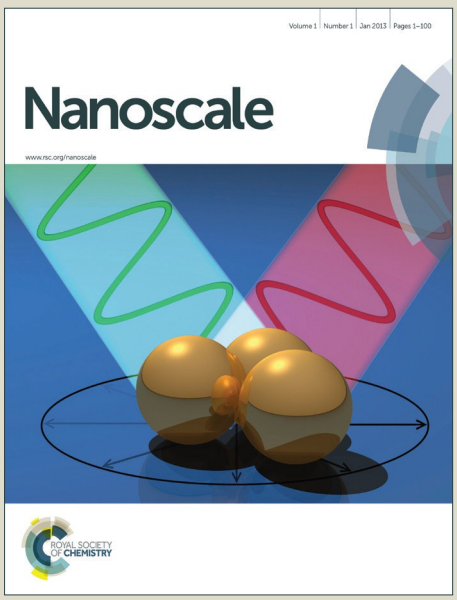

ROYAL SOCIETY OF CHEMISTRY

www.rsc.org/nanoscale

Nanoscale

ARTICLE

An amphiphilic graft copolymer-based nanoparticle platform for reduction-responsive anticancer and antimalarial drug delivery

Received 00th January 20xx,
Accepted 00th January 20xx

DOI: 10.1039/x0xx00000x

www.rsc.org/chemicalscience

Adrian Najer,[‡abc] Dalin Wu,[‡a] Martin G. Nussbaumer,[a] Geoffrey Schwertz,[d] Anatol Schwab,[d] Matthias C. Witschel,[e] Anja Schäfer,[bc] François Diederich,[d] Matthias Rottmann,[bc] Cornelia G. Palivan,[a] Hans-Peter Beck[bc] and Wolfgang Meier[*a]

Medical applications of anticancer and antimalarial drugs often suffer from low aqueous solubility, high systemic toxicity, and metabolic instability. Smart nanocarrier-based drug delivery systems provide means of solving these problems at once. Herein, we present such a smart nanoparticle platform based on self-assembled, reduction-responsive amphiphilic graft copolymers, which were successfully synthesized through thiol-disulfide exchange reaction between thiolated hydrophilic block and pyridyl disulfide functionalized hydrophobic block. These amphiphilic graft copolymers self-assembled into nanoparticles with mean diameters of about 30 – 50 nm and readily incorporated hydrophobic guest molecules. Fluorescence correlation spectroscopy (FCS) was used to study nanoparticle stability and triggered release of a model compound in detail. Long-term colloidal stability and model compound retention within the nanoparticles was found when analyzed in cell media at body temperature. In contrast, rapid, complete reduction-triggered disassembly and model compound release was achieved within a physiological reducing environment. The synthesized copolymers revealed no intrinsic cellular toxicity up to 1 mg/mL. Drug-loaded reduction-sensitive nanoparticles delivered a hydrophobic model anticancer drug (doxorubicin, DOX) to cancer cells (HeLa cells) and an experimental, metabolically unstable antimalarial drug (the serine hydroxymethyltransferase (SHMT) inhibitor (±)-**1**) to *Plasmodium falciparum*-infected red blood cells (iRBCs), with higher efficacy compared to similar, non-sensitive drug-loaded nanoparticles. These responsive copolymer-based nanoparticles represent a promising candidate as smart nanocarrier platform for various drugs to be applied to different diseases, due to the biocompatibility and biodegradability of the hydrophobic block, and the protein-repellant hydrophilic block.

Introduction

Nanoparticle-assisted drug delivery allows for tuning pharmacokinetics, toxicity, absorption, distribution, metabolism, and excretion profile of drugs leading to different needs for dosage and duration of treatment.[1] This concept has been widely applied for improving clinical outcome of anticancer therapy through increasing drug accumulation at the target site while decreasing drug distribution to off-target sites.[2,3] Passive targeting of tumor tissue can be obtained using non-functionalized, drug-loaded nanoparticles via the enhanced permeability and retention (EPR) effect, which allows nanoparticle accumulation in tumors after intravenous application.[4,5] In terms of size, passive accumulation within tumor tissue via the EPR effect is efficiently achieved with long-circulating nanoparticles ranging from 10 to 100 nm in diameter.[6] However, small sized nanoparticles (sub-50 nm diameter) have been shown to better target *e.g.* lymph node metastatic cancer.[7]

Amphiphilic block copolymer (ABP)-based nanomaterials are one promising type of materials with broad applicability in drug delivery.[2,3] Various self-assembled nanostructures ranging from micelles to worm-like micelles to polymer vesicles can be obtained in aqueous environments by carefully choosing the type, architecture, lengths, and hydrophilic/hydrophobic block ratio of ABPs.[8-10] ABP-based nanoparticles benefit from lower critical micelle concentrations (CMC), higher mechanical stability, simple introduction of stimuli-responsiveness within the ABP architecture, and modification with targeting moieties when compared to lipid based systems such as liposomes.[3,11,12] Degradability of ABP-based nanoparticles is introduced by using polypeptides, polyphosphoesters, or polyesters, such as poly(ε-caprolactone) (PCL), as ABP hydrophobic building blocks.[13,14] Poly(ethylene glycol) (PEG) is the most readily used

[a] Department of Chemistry, University of Basel, Klingelbergstrasse 80, CH-4056 Basel, Switzerland. E-mail: wolfgang.meier@unibas.ch; Tel: +41 (0)61 267 38 02
[b] Swiss Tropical and Public Health Institute, Socinstrasse 57 Postfach, CH-4002 Basel, Switzerland.
[c] University of Basel, Petersgraben 2, CH-4002 Basel, Switzerland.
[d] Laboratorium für Organische Chemie, ETH Zurich, Vladimir-Prelog-Weg 3, 8093 Zurich, Switzerland.
[e] BASF SE, Carl-Bosch-Strasse 38, 67056 Ludwigshafen, Germany.
‡Equal contribution.
†Electronic Supplementary Information (ESI) available: Detailed experimental procedures, additional schemes and supplementary data including NMR, FTIR, TEM, DLS, UV-Vis, FCS, and fluorescence microscopy images. See DOI: 10.1039/x0xx00000x

polymer for the hydrophilic part of ABPs, due to the biocompatibility and non-fouling properties of this polymer, needed for achieving long-circulating nanoparticles.[15] However, injection of PEG-based nanostructures can induce an immune response against PEG.[16] This significantly reduces the efficacy of a PEG-based drug delivery system, specifically for repeated administration,[16] which highlights the urgent need for alternative hydrophilic blocks to be exposed on drug delivery vehicles.[15,17,18]

Another challenging aspect of nanoparticle-based drug delivery is the efficient release of the drug in the target cell, while retaining the drug inside the nanostructure in the extracellular environment. This is elegantly addressed by spatiotemporal- and dosage-controlled delivery using stimuli-responsive materials and corresponding nanostructures.[19-21] Commonly used endogenous triggers for stimuli-responsive delivery are changes in pH, redox potential, and enzyme concentration.[19] Reduction-responsive ABP-based nanoparticles represent a unique class of smart materials based on their effective delivery mechanism for a wide range of molecules, such as nucleic acids[22,23] and low molecular weight chemical drugs.[24-27] The building blocks of these nanostructures contain one or more disulfide linkage/s in their main- or side-chains. This allows forming drug-loaded nanoparticles with stable morphology in circulation and extracellular environments. After cellular uptake, rapid cleavage of the disulfide linkage/s and subsequent nanoparticle disassembly in the reductive cell cytosol promote drug release.[28] The large gradient of the reducing agent glutathione (GSH) across cell membranes – the cytosolic concentration (2 – 10 mM) is three orders of magnitude higher than the extracellular concentration – serves as the basis for reduction-responsive anticancer drug delivery.[29]

Solubility, stability and toxicity problems are well known for anticancer drugs,[30] but the same problems equally apply to anti-infectious agents, such as antimalarials.[31,32] Malaria is an infectious disease caused by *Plasmodium* spp. parasites, transmitted by *Anopheles* mosquitos. The disease causing stages of the parasite infect and asexually divide inside of human red blood cells (RBCs).[33] The need for novel antimalarials or strategies against resistance development is increasingly recognized. Especially since the recent development and spread of resistance against the first-line treatment with artemisinin combination,[34] which already led to treatment failures.[35] One proposed approach to overcome the development of resistance is the delivery of high local concentrations of antimalarials using *e.g.* nanoparticles.[36,37] Current antimalarial drug delivery strategies are focused on commercial antimalarials that have already been optimized for *in vivo* applications.[38,39]

Surprisingly, there is evidence that proteins, such as antibodies,[40] and small nanoparticles up to about 80 nm diameter have direct access to the parasite inside the RBC.[36,41,42] Several mechanisms for specific uptake of large molecules and nanoparticles by parasitized RBCs compared to RBCs have been proposed,[43] but this is an ongoing controversy. Similarly to passive tumor targeting via the EPR effect, this controversial "leakiness" of *Plasmodium*-infected RBCs (iRBCs)[36,41,42] can be exploited via a passive targeting strategy using non-functionalized, antimalarial-loaded nanoparticles. Also here, smaller sized nanoparticles (sub-80 nm diameter) are needed, because the size-cutoff to efficiently reach intracellular malaria parasites of iRBCs is about 80 nm.[36,41,42] The highly reducing parasite cytosol of iRBCs[44] equally represents a valuable trigger for smart drug delivery of antimalarials via reduction-triggerable nanoparticles, similar to reduction-triggered anticancer drug delivery. Additionally, drug-resistant intracellular malaria parasites were reported to possess even further increased cytosolic reduction potentials.[45,46]

Herein, we introduce a novel, alternative type of ABP-based nanoparticles using a PEG-alternative, poly(2-methyl-2-oxazoline) (PMOXA), as the hydrophilic block. Specifically, we report the synthesis of a library of biodegradable, reduction-responsive ABPs composed of hydrophilic PMOXA and hydrophobic PCL with grafted molecular architecture, poly(2-methyl-2-oxazoline)-*graft*(SS)-poly(ε-caprolactone) (PMOXA-*g*(SS)-PCL), in which the reduction-responsive disulfide group acts as the linker between PMOXA and PCL. Aqueous self-assembly of these graft copolymers into nanoparticles and loading of cargo using model hydrophobic dye molecules (Bodipy630, NileRed), anticancer drug (doxorubicin, DOX), and antimalarial (serine hydroxymethyltransferase (SHMT) inhibitor (±)-**1**)[32] were studied (Scheme 1). A single molecule detection method, fluorescence correlation spectroscopy (FCS), was used to demonstrate high stability and model dye retention within self-assembled nanoparticles in protein-containing cell media over four days and fast disassembly and model compound release upon treatment with reducing agent. Furthermore, the biocompatibility of these copolymers was tested on HeLa cells in the range of 0.1 mg/mL to 1 mg/mL. Anticancer drug-loaded reduction-sensitive nanoparticles were evaluated for delivery of their payload to cancer cells (Hela) and compared to non-sensitive nanoparticles based on similar polymers with linear architecture, PMOXA-*b*-PCL. Similarly, we explored the nanoparticle-based delivery of a non-optimized, hydrophobic, and metabolically unstable antimalarial compound, which is in preclinical drug development stage, to

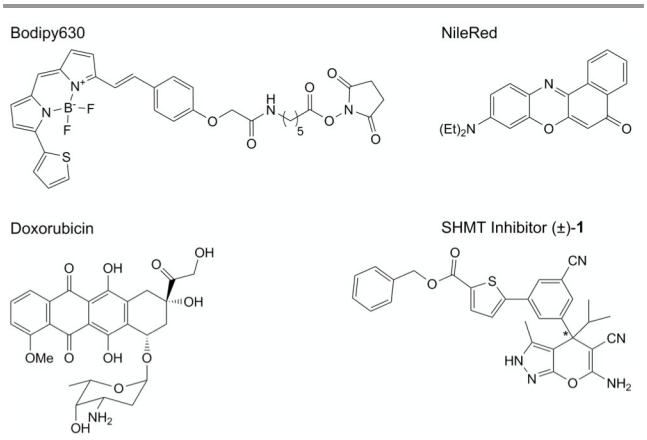

Scheme 1 Chemical structures of model hydrophobic cargo molecules used for incorporation in nanoparticles.

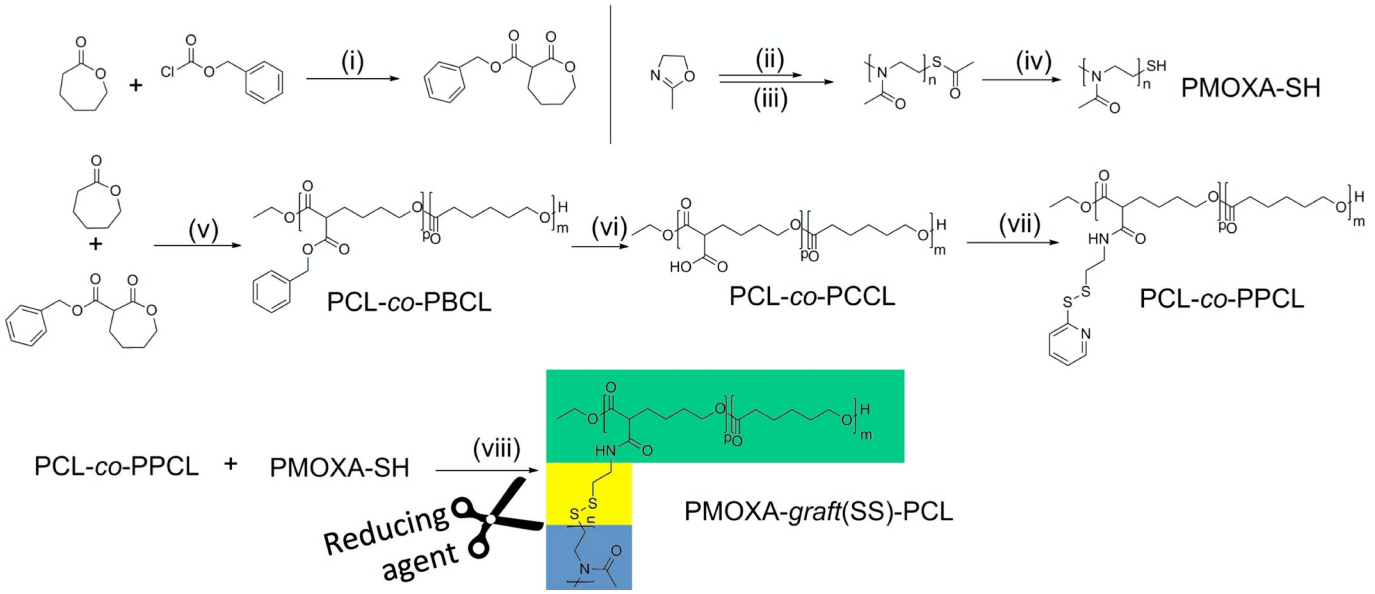

Scheme 2 The synthetic route for PMOXA-SH, PCL-*co*-PPCL, and PMOXA-*g*(SS)-PCL. Reagents and conditions: (i) *n*-butyllithium solution (2.5 M in hexanes), benzyl chloroformate, $LiAlH_4$, THF, –75 °C for 3 h under argon; (ii) methyl trifluoromethanesulfonate, 2-methyl-2-oxazoline, acetonitrile, 80 °C for 24 h under argon; (iii) potassium thioacetate, RT for 24 h under argon (yield: 92%); (iv) triphenylphosphine, anhydrous MeOH, RT for 48 h under argon (yield: 85%); (v) anhydrous EtOH, ε-caprolactone, α-benzyl carboxylate-ε-caprolactone, Zn(II) 2-ethylhexanoate, toluene, 110 °C for 24 h under argon (yield: 82%); (vi) Pd/C (10 wt. %), ethyl acetate, RT for 42 h under hydrogen (yield: 85%); (vii) 2-pyridylthiol cysteamine hydrochloride, *N,N'*-dicyclohexylcarbodiimide (DCC), 4-dimethylaminopyridine, triethylamine, CH_2Cl_2, RT for 60 h under argon (yield: 60%); (viii) PMOXA-SH, PCL-*co*-PPCL, acetic acid, DMF, RT for 60 h under argon (yield: 38%). The yellow-labeled disulfide bridge represents the reduction-responsive chemical group connecting hydrophobic (green) and hydrophilic block (blue).

iRBCs. The trigger for nanoparticle disassembly and antimalarial release is the highly reducing cytosol of intracellular parasites. We consider this nanoparticle-assisted delivery as a valuable additional avenue to medicinal chemistry traditionally used to modify pharmacokinetic properties of compounds via changing the chemical structure of the compound itself.

Results and discussion

Graft copolymer synthesis and characterization

A novel graft copolymer was designed and synthesized based on PMOXA hydrophilic polymer and PCL hydrophobic polymer (Scheme 2) to provide a reduction-sensitive, biodegradable building block for a nanoparticle platform to deliver anticancer and antimalarial drugs via a triggered release mechanism.

PMOXA is considered a strong alternative to PEG,[15,18,47-49] which has mainly been used as hydrophilic block in ABPs, but more recently, problems arose *e.g.* due to immune response after repeated administration of PEG-based systems.[16] This highlights the urgent need for alternative copolymers for drug delivery. The design of our graft copolymer has been inspired by previous works that have demonstrated synthesis of biodegradable, readily modifiable random copolymer of poly(ε-caprolactone)-*co*-poly(α-carboxyl-ε-caprolactone) (PCL-*co*-PCCL)[50] and pyridyl disulfide-functionalized biodegradable polymers to form reduction-sensitive copolymers via thiol-disulfide exchange reaction.[51] In the present work, we first synthesized thiolated PMOXA (PMOXA-SH) through living ring-opening polymerization of 2-methyl-2-oxazoline and end group functionalization,[17] which was then coupled via thiol-disulfide exchange reaction with pyridyl disulfide functionalized poly(ε-caprolactone) (PCL-*co*-PPCL) to obtain the desired graft copolymer with reduction-responsive disulfide connection of hydrophobic and hydrophilic blocks.

Three PMOXA-*g*(SS)-PCL copolymers with different molecular ratio (hydrophilic fraction, $f_{(PMOXA)}$) and molecular weights were synthesized (Table 1). A reduction-insensitive copolymer PMOXA-*b*-PCL was synthesized additionally to form non-triggered, biodegradable nanoparticles (Scheme S1, Fig. S5). Detailed experimental procedures and polymer characterization can be found in the Supplementary Information.

The appearance of the peaks at 2.34 ppm and 2.94 ppm in the ^{1}H NMR spectrum ($(CD_3)_2SO$) belonging to the protons on methyl group of thiolacetate and methylene group next to the thiol group indicated the successful reaction with potassium thioacetate to obtain PMOXA-SAc (Fig. S1A).[52] PMOXA-SAc was further activated by PPh_3 in anhydrous MeOH to yield PMOXA-SH, which was confirmed by the disappearance of the peaks at 2.34 ppm (Fig. S1B). Fast manipulation was necessary to avoid disulfide formation during the purification steps.

The hydrophobic, biodegradable PCL-based copolymer part with anchor points for hydrophilic polymers was synthesized based on a modified protocol.[50] The appearance of ^{1}H NMR signals at 5.23 ppm and 7.26 ppm belonging to the protons on the methylene group next to benzyl group and protons on the benzyl group demonstrated successful random copolymerization of α-benzyl carboxylate-ε-caprolactone and ε-caprolactone yielding poly(ε-caprolactone)-*co*-poly(α-benzyl carboxylate-ε-caprolactone) (PCL-*co*-PBCL, Fig. S2B). The corresponding molecular weights and dispersities (Đ), as

Table 1 Chemical characteristics of PCL-*co*-PBCLs and PMOXA-*g*(SS)-PCLs.

	^{1}H NMR			GPC			CMC
Polymer	Block ratio	*Mn*	$f_{(PMOXA)}$ [a]	*Mw*	*Mn*	Đ	mg/mL
PCL-*co*-PBCL **1**	264:13	33360	–	40000	19400	2.0	–
PCL-*co*-PBCL **2**	126:3	15150	–	13000	19670	1.50	–
PMOXA-*g*(SS)-PCL **2**	88:238	34800	22%	22300	13000	1.72	$0.05*10^{-3}$
PMOXA-*g*(SS)-PCL **1**	127:165	30000	36%	18400	13260	1.38	$0.20*10^{-3}$
PMOXA-*g*(SS)-PCL **3**	135:135	27000	43%	–[b]	–	–	$0.29*10^{-3}$

[a] The values of $f_{(PMOXA)}$ were calculated by the equation $\frac{Mn\ of\ PMOXA}{Mn\ of\ whole\ copolymer}$

[b] Due to solubility problems of PMOXA-*g*(SS)-PCL **3** in THF, no GPC data were obtained.

determined by ^{1}H NMR and gel permeation chromatography (GPC) for two PCL-*co*-PBCLs, are listed in Table 1. Subsequently, PCL-*co*-PBCL was reduced by Pd/C under hydrogen atmosphere to obtain PCL-*co*-PCCL as monitored by the disappearance of the signals at 5.23 ppm and 7.26 ppm belonging to the benzyl groups (Fig. S2B).[50] Finally, the PCL-*co*-PCCL was reacted with 2-pyridylthio cysteamine hydrochloride in presence of DCC as coupling agent to yield PCL-*co*-PPCL, which was demonstrated by the appearance of peaks at 2.93 ppm (methylene protons next to the disulfide group) and 7.0–8.6 ppm (protons of the pyridyl group) (Fig. S2C).

PMOXA-SH, PCL-*co*-PPCL, and a catalytic amount of acetic acid[51] were subsequently used to synthesize the final reduction-sensitive amphiphilic graft copolymers PMOXA-*g*(SS)-PCL through a thiol-disulfide exchange reaction. After precipitating the product in cold MeOH to remove unreacted PMOXA-SH, the coappearance of characteristic proton signals of PMOXA and PCL indicated the successful synthesis of the desired graft copolymer (Fig. S3). The signal at 2.84 ppm corresponds to the protons on the carbon next to the disulfide, which confirmed the reduction-sensitive linkage within the graft copolymer. FT-IR was used to further characterize the synthesized polymers and copolymers (Fig. S4). The absorbance bands at 1720 cm^{-1} and 1160 cm^{-1} in the FT-IR spectrum of PMOXA-*g*(SS)-PCL were assigned to stretching vibration of C=O and C-O on PCL, and the band at 1634 cm^{-1} is the characteristic vibration of C=O on PMOXA, additionally indicating successful synthesis of PMOXA-*g*(SS)-PCL copolymers. Interestingly, the molecular weight of PMOXA-*g*(SS)-PCL **1** and PMOXA-*g*(SS)-PCL **2** determined from ^{1}H NMR were higher compared to GPC data, which might be caused by the grafted structure of the copolymer.[51]

Self-assembly and reduction-triggered disintegration of PMOXA-*g*(SS)-PCL nanoparticles

Nanoparticles were self-assembled from reduction-sensitive PMOXA-*g*(SS)-PCLs graft copolymer to yield a triggerable nanoparticle platform for the delivery of active compounds. The solvent switch method was used for preparation of nanoparticles by dropwise addition of phosphate buffered saline (PBS) to stirred organic solutions (DMF) containing dissolved graft copolymer. Subsequently, self-assembly was finalized and samples were purified by extensive dialysis in aqueous solutions (physiological saline solution or PBS). The obtained mean diameters of the self-assembled, reduction-sensitive nanoparticles in PBS ranged from about 27 nm to 51 nm with narrow PDI of 0.09 to 0.18 for all three graft copolymers according to dynamic light scattering (DLS) measurements in PBS (Fig. 1C). Transmission electron micrographs (TEM) confirmed the size and morphology of the assembled spherical nanoparticles (Fig. 1B, S6). These obtained nanoparticle sizes lie within the optimum range of 10 to 100 nm to be used as passively targeted drug delivery vehicles.[6] The relatively small average size of maximum 50 nm provides the basis for targeting cancer metastasis[7] and iRBCs in case of malaria.[36,41,42]

Interestingly, the average diameter of self-assembled nanoparticles decreased with increasing hydrophilic content ($f_{(PMOXA)}$, Fig. 1C). This decrease can be attributed to the fact that PMOXA-*g*(SS)-PCL copolymers with higher $f_{(PMOXA)}$ have higher interfacial curvature values, which pushes the self-assembly towards smaller structures.[8,9] The CMC in PBS was measured using pyrene as a fluorescent probe (Table 1 and Fig. S7).[53] The CMC values increased with increasing fraction of

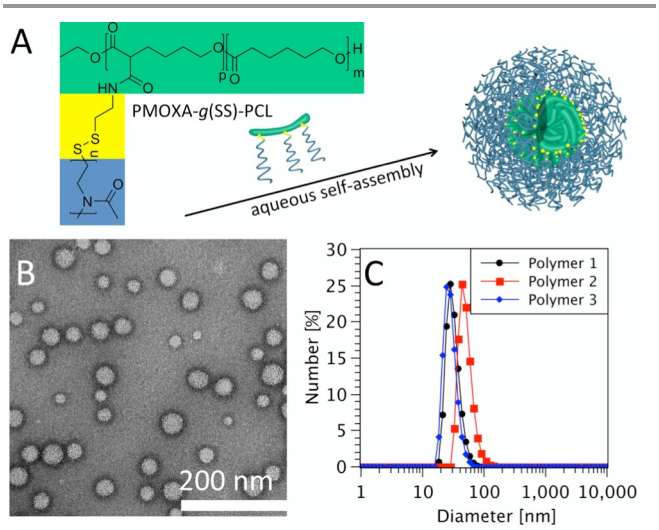

Fig. 1 (A) Chemical structure of PMOXA-*g*(SS)-PCL and schematic self-assembly in aqueous solution. (B) Morphology of nanoparticles self-assembled from PMOXA-*g*(SS)-PCL **2** imaged by transmission electron microscopy (TEM). (C) Hydrodynamic diameter and number distribution of nanoparticles in PBS measured by DLS. More TEM images, and DLS size distributions of nanoparticles self-assembled from PMOXA-*g*(SS)-PCL **1**, PMOXA-*g*(SS)-PCL **3**, and linear PMOXA-*b*-PCL are shown in Fig. S6, S10, S12, S13.

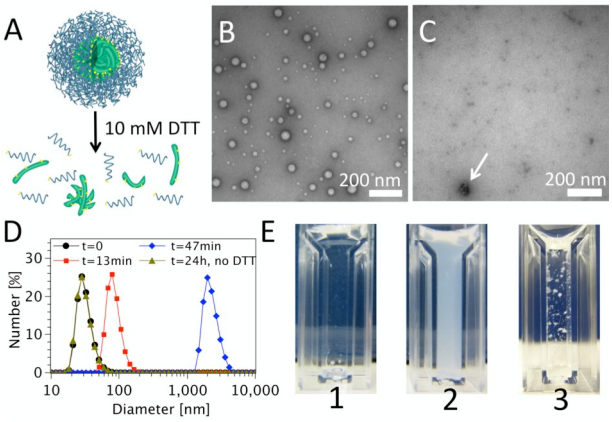

Fig. 2 Reduction triggered disassembly of PMOXA-*g*(SS)-PCL nanoparticles. (A) Schematic disassembly process showing the cleavage of the disulfide bonds leading to free PMOXA-SH (blue) and PCL (green). (B) TEM of PMOXA-*g*(SS)-PCL **1** nanoparticles after incubation in PBS at 37 °C for 31 h. (C) TEM image of the same sample after incubation in PBS containing 10 mM DTT at 37 °C for 31 h. The white arrow indicates a PCL aggregate (1H NMR, Fig. S8). (D) Changes in diameter of nanoparticles self-assembled from PMOXA-*g*(SS)-PCL **1** in time response to 10 mM DTT as measured by DLS; only in the presence of DTT the diameter rapidly shifted to very large values (red, blue curve), at time point 0 (black curve) and after incubation without DTT for 24 h (green curve) the nanoparticles appeared similarly. (E) Digital images of nanoparticle solution formed by PMOXA-*g*(SS)-PCL **1** (1 mg/mL) in DLS cuvettes in a time series after 10 mM DTT treatment. (1) 13 minutes, (2) 47 minutes, and (3) 4 h.

hydrophilic domains, which is in agreement with previous literature.[9] These CMC values are in general several orders of magnitude lower compared to CMC values for low molecular weight surfactants indicating much higher stability upon dilution, which is desirable for long circulation and drug retention within the nanocarrier after dilution in the bloodstream.[11]

DLS was further used to investigate the reduction sensitivity of PMOXA-g(SS)-PCL **1** self-assembled nanoparticles by addition of 10 mM reducing agent dithiothreitol (DTT) in PBS, which is a standard method and concentration used in the field.[54] This mimics the physiological cytosolic concentration of reducing agent (10 mM GSH) found in the reducing cytosol of cancer cells.[29] Similarly, intracellular malaria parasites possess a highly reducing cytosol.[44] DLS results demonstrated that nanoparticles remained stable for at least 24 hours in the absence of reducing agent, but were quickly destabilized by reducing agent (Fig. 2).

The diameter of reduction-sensitive nanoparticles rapidly increased after incubation in a physiological reducing environment (Fig. 2D), which was even apparent by eye due to the increase in turbidity and subsequent formation of white precipitation (Fig. 2E). We speculated that these white macroscopic precipitates (Fig. 2E-3) have resulted from aggregation of insoluble PCL after cleavage of hydrophilic blocks (PMOXA) from the copolymers. ^{1}H NMR confirmed this theory, because we exclusively measured proton signals characteristic for PCL, after filtering and washing the obtained precipitate in MeOH (Fig. S8). These results clearly indicate that the disulfide bridge between PMOXA and PCL was reduced in the presence of DTT, which led to disintegration of nanoparticles. Additionally, TEM images confirmed nanoparticle stability at 37 °C for at least 31 h (Fig. 2B). In the presence of reducing agent nanoparticles disassembled – they were not visible in TEM images anymore – and only few polymer aggregates remained (Fig. 2C, white arrow points to one aggregate). This nanoparticle design allows reduction-triggered disassembly, subsequent degradation of remaining hydrophobic polyester blocks (PCL) over time, and excretion of hydrophilic PMOXA chains via kidneys, as *e.g.* demonstrated for similar PEG chains up to 30 kDa,[55] demonstrating the suitability of these copolymers for biomedical applications. Furthermore, our nanoparticle platform provides an alternative to PEG-based nanoparticles, which are currently being proposed for many drug delivery applications, but these need to be replaced by other types due to adverse effects after repeated administration of structures based on PEG.[16]

Loading of various hydrophobic model molecules within nanoparticles

Various hydrophobic cargo molecules were chosen to be incorporated within the hydrophobic core of self-assembled nanostructures for stabilization and protection purposes. The fluorescent dye molecules Bodipy630 and NileRed, the anticancer drug doxorubicin (DOX), and the experimental, metabolically unstable antimalarial (SHMT inhibitor (±)-**1**)[32] were the selected compounds for encapsulation in nanoparticles formed by reduction-sensitive PMOXA-*g*(SS)-PCLs and PMOXA-*b*-PCL. Non-triggered PMOXA-*b*-PCL-based nanoparticles served as biodegradable, but reduction insensitive control nanostructures. All these hydrophobic molecules were readily incorporated into the hydrophobic core of all the different nanoparticles. Drug loading efficiencies (DLE) of 15%, 30%, 40%, and 55% for NileRed, Bodipy630, DOX, and SHMT inhibitor (±)-**1**, respectively, were measured by fluorescence (DOX, Fig. S9) and UV-Vis absorbance (dyes and antimalarial, Fig. S11) measurements for reduction-sensitive nanoparticles. DLS measurements of drug/dye-loaded nanoparticles revealed typical average diameters of 42 ± 11 nm for reduction-sensitive nanoparticles and 74 ± 24 nm for similar, non-sensitive nanoparticles (Fig. S10, S13). TEM images confirmed these sizes (Fig. S12, S13).

Encapsulation of one model compound (DOX) was studied in more detail (Table S1). Nanoparticles from all three PMOXA-*g*(SS)-PCL **1** –**3** were loaded with various DOX feeding amounts and with theoretical drug loading contents (DLC) of 4.8 wt%, 13 wt% and 20 wt%. Interestingly, the DLEs were always around 40% for all the samples, which indicated that the theoretical DLCs and the difference of polymer chemical structure had very little influence on DLE (Table S1). The 40% DLE was slightly lower than the values (DLE > 50%) reported for nanoparticles based on cross-linked polyurethane micelles (CCL-PUMs) and PCL-*g*-SS-PEG copolymers (^{1}H NMR: 35600 g/mol–66000 g/mol),[24,51] which is explained by the non-crosslinkable structure and lower molecular weight molecular structure of our PMOXA-*g*(SS)-PCLs. However, our copolymers

are synthesized via a simpler synthesis route, which would overcompensate for a slightly lower DLE. Our results further demonstrated that the nanoparticles were loaded with more drugs (DLC increases) when more drugs were fed (Table S1). In this respect, the final diameters and polydispersity indices (PDI) of DOX-loaded nanoparticles slightly increased with increasing drug feed for all three PMOXA-*g*(SS)-PCL copolymers (Table S1 and Fig. S10), which was caused by more encapsulated DOX occupying more spatial area in the nanoparticle core, which is in agreement with previously reported results.[51]

Reduction-triggered model compound release and stability of nanoparticles in cell media

The design of smart drug delivery vehicles demands for stable nanostructures, which do not aggregate, keep the drug within the carrier prior to cellular uptake, and subsequently release the payload upon reaching cellular compartments that provide the desired trigger. FCS is a method that allows to study dye encapsulation, stability and triggered release on a single molecule level.[56,57] FCS was used herein to first follow the reduction-triggered disintegration of reduction-responsive nanoparticles formed from PMOXA-*g*(SS)-PCLs and release behavior of a model hydrophobic cargo (Bodipy630) upon treatment with reducing agents (DTT or GSH) at physiological concentrations. It can be determined whether the dye is encapsulated or freely diffusing by following the diffusion times (τ_D) of fluorescent molecules. Time series of FCS curves were recorded in the presence or absence of reducing agent to follow reduction-triggered model compound release from triggered nanoparticles compared to a non-triggered nanoparticle version (Fig. 3, S14). The fraction of free dye versus encapsulated dye was followed using a two-component fit of the obtained autocorrelation curves (Fig. 3A). Simultaneously, the hydrodynamic diameters of the nanoparticles and the number of dye molecules per single nanoparticle were calculated from the diffusion times (τ_D) and molecular brightness (counts per molecule, CPM in kHz), respectively, by comparing values of nanoparticles to values obtained for free dye. The obtained nanoparticle hydrodynamic diameters using FCS (Fig. 3B, S14C, S15) are in good agreement with values measured by DLS and TEM (Fig. 1, S10, S12, S13). Furthermore, the reducing agent-induced increase of nanoparticle sizes for the reduction-sensitive copolymers was confirmed by FCS (Fig. S14).

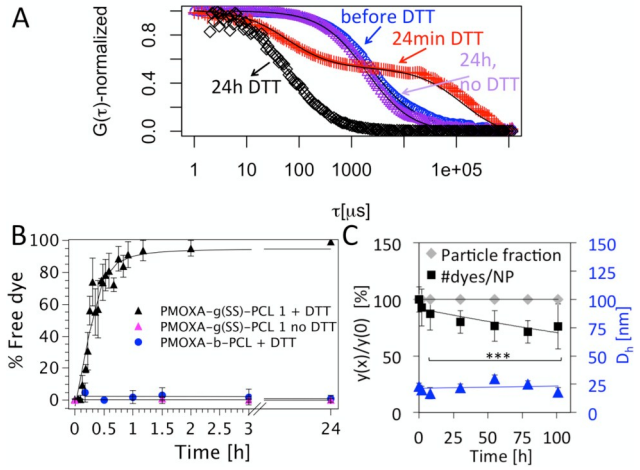

Fig. 3 Reduction-triggered disassembly and dye release from PMOXA-*g*(SS)-PCL nanoparticles and nanoparticle cell medium stability studied by fluorescence correlation spectroscopy (FCS). (A) Normalized autocorrelation curves (symbols) and fits (lines) from FCS measurements using Bodipy630-loaded PMOXA-*g*(SS)-PCL **1** nanoparticles in absence and presence of 10 mM DTT in PBS: t = 0 min (blue circles, 0% free dye fraction), t = 24 min (red crosses, 46% free dye fraction), t = 24 h (black diamonds, 100% free dye fraction), t = 24 h without DTT (magenta triangles, 0% free dye fraction). (B) Time series of the percentage of free dye fraction from FCS curves of nanoparticles in PBS with/without 10 mM DTT at 37 °C. Free dye was only appearing for PMOXA-*g*(SS)-PCL in presence of DTT, whereas incubation in PBS or non-sensitive PMOXA-*b*-PCL-nanoparticles in 10 mM DTT did not show free dye up to 24 h incubation. Values are mean of three independent measurements ± SEM for each time point. (C) Stability of PMOXA-*g*(SS)-PCL **3** Bodipy630-loaded nanoparticles in malaria culture medium (MCM) at 37 °C under shaking conditions for four days; nanoparticle fraction from two-component autocorrelation curve fitting compared to time point 0 (grey diamonds), change in number of dye molecules per nanoparticles calculated from molecular brightness (CPM) data compared to time point 0 (black squares), and hydrodynamic nanoparticle diameter (D_h) calculated from obtained diffusion times (blue triangles). Data for the other copolymers, time series of nanoparticle D_h in presence or absence of DTT, and stability in both cancer cell medium and MCM can all be found in SI (Fig. S14, S15). Values are mean of 30 curves ± SD at each time point. Statistics was analyzed using two-tailed Student's *t*-test.

The reduction-triggered release of a model cargo (Bodipy630) from all reduction-sensitive nanoparticles compared to stable, non-sensitive nanoparticles was successfully achieved as demonstrated by FCS measurements (Fig. 3A,B, S14A,B,D). The free dye population obtained from two component fits was only increasing over time – reaching more than 90% free dye after 1.5 h – in case of PMOXA-*g*(SS)-PCL nanoparticles in the presence of DTT (10 mM). The release from PMOXA-*g*(SS)-PCL nanoparticles was slower when the physiological reducing agent GSH (10 mM) was used (7 h to reach about 90% free dye, Fig. S14D). This is explained by the weaker reducing potential of GSH compared to DTT[58] and the formation of glutathione disulfides (GSSG) in buffer. However, intracellular conditions are much more complex, including other redox molecules, many proteins/enzymes including glutathione reductase, which maintains the reducing potential within the cell cytosol.[59]

The same PMOXA-*g*(SS)-PCL nanoparticles samples incubated without reducing agent or non-sensitive nanoparticles (PMOXA-*b*-PCL) with reducing agent (10 mM DTT or GSH) did not reveal a free dye population in FCS curves even after 24 h. This smart compound release from nanoparticles at physiological, cytosolic reducing agent concentration at 37 °C sets the basis for triggered delivery of hydrophobic and unstable drug molecules to cancer cells and malaria parasite infected RBCs.

Before cell experiments were conducted, the stability of the loaded nanocarriers was studied in detail on a single molecule level using FCS. These measurements were performed at physiological temperature (37 °C) under shaking conditions in the complete cell media (containing proteins), which were subsequently used for assays with cancer cells and malaria

parasites. Reduction-sensitive and non-sensitive nanoparticles were both highly stable in terms of nanoparticle size, colloidal stability, and dye retention within the nanoparticles in both cell media for the whole tested time window of four days, which was the maximum incubation time used in cell assays (Fig. 3C, S15). Overall, all the nanoparticle samples did not reveal any dye release throughout the whole assay time as calculated from two component fits of autocorrelation curves, which did not yield any significant fractions of fast diffusing species (grey diamonds, Fig. 3C, S15). The diffusion time of this fast diffusing component was fixed to typical values of about 300 µs, which is different to free dye diffusion due to interaction of media proteins with hydrophobic dye molecules as calibrated by FCS of dye in complete cell media. An average of 18% and 2% dye release was calculated at the end of the four-day assay in case of reduction-sensitive and non-sensitive nanoparticles, respectively, when comparing the change in the number of dye molecules per nanoparticle, via CPM comparison of free dye to nanoparticle values over time. But these small differences compared to time point zero were mostly not significant (Fig. S15). The nanoparticle hydrodynamic diameters (D_h) remained similar for all samples over the whole time course of four days, remaining in the optimal size window of D_h = 10 to 100 nm needed for optimal drug delivery via passive targeting.[6] This was expected due to the protein-repellant PMOXA[15,18] hydrophilic blocks exposed on the nanoparticle surfaces. This is an important aspect, since nanoparticle aggregation would significantly hamper accessibility of nanoparticles to tumor sites and iRBCs. Blood circulation times *in vivo* – needed for efficient passive accumulation of the drug-loaded nanoparticles at tumor sites or within iRBCs – would also be reduced due to increased hepatosplenic filtration. This demonstrates the high potential of triggered nanoparticles based on PMOXA hydrophilic blocks that can be seen as valuable alternatives to overcome problems associated with PEG-based nanoparticles.[16]

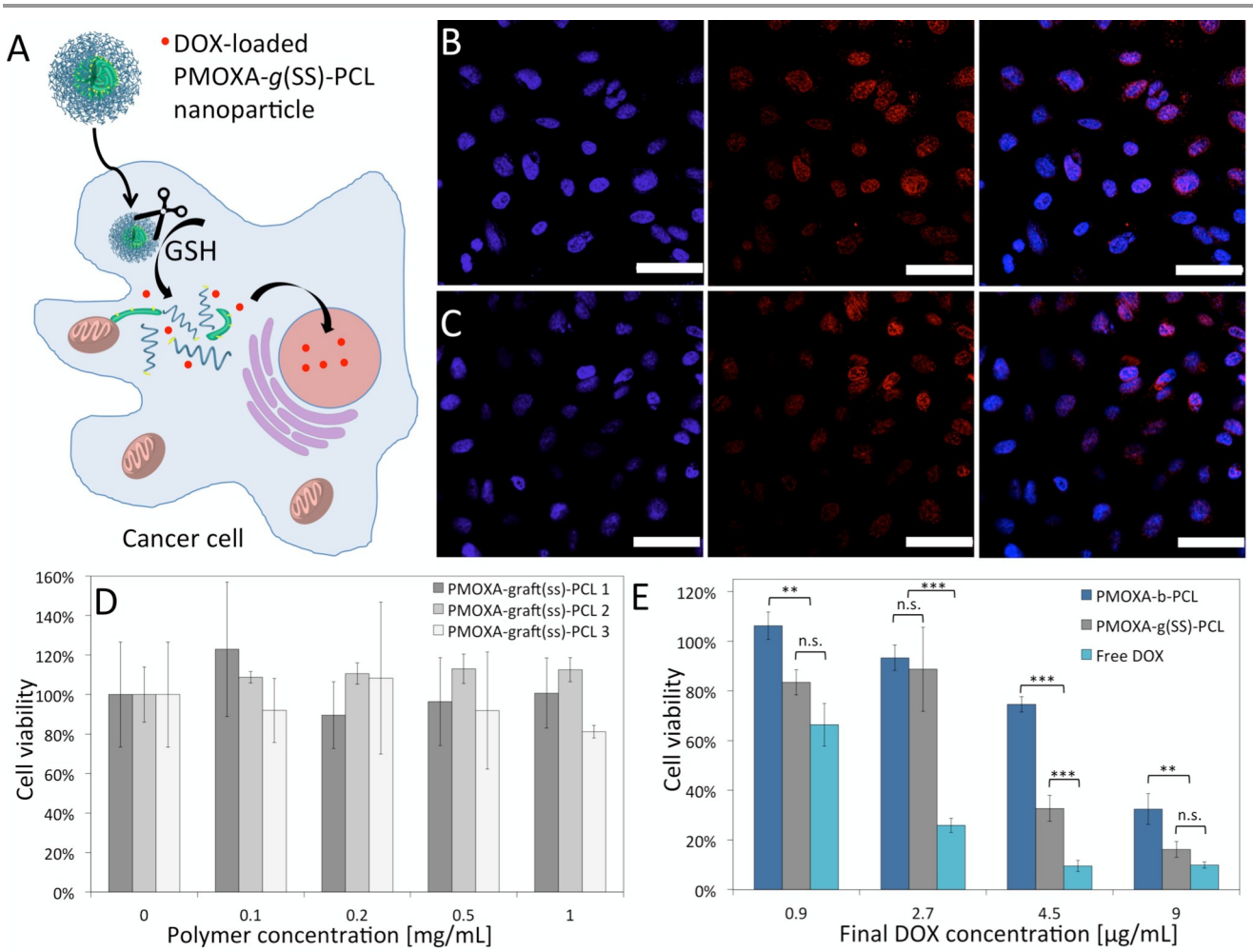

Fig. 4 Polymer biocompatibility, uptake and release of DOX from DOX-loaded reduction-sensitive PMOXA-*g*(SS)-PCL nanoparticles. (A) Schematic process of nanoparticle uptake and reduction-triggered (GSH) disassembly of nanoparticles and drug release. (B, C) CLSM images of intracellular DOX release from the reduction-responsive, DOX-loaded PMOXA-*g*(SS)-PCL **2** nanoparticles using HeLa cells after 1 h of incubation. For each panel, images from left to right show cell nuclei stained by Hoechst 33342 (blue), DOX fluorescence in cells (red) and overlays of the two images. (B) DOX loaded PMOXA-*g*(SS)-PCL **2** nanoparticles (0.25 µg/mL DOX), (C) free DOX as control (0.25 µg/mL DOX). Scale bars are 50 µm. (D) Viabilities of HeLa cells after incubation with empty PMOXA-*g*(SS)-PCL nanoparticles for 48 h demonstrating absence of apparent polymer toxicity. All the data are presented as average ± SD (n = 4). (E) Viability of HeLa cells incubated with DOX-loaded PMOXA-*g*(SS)-PCL nanoparticles, DOX-loaded PMOXA-*b*-PCL nanoparticles, and free DOX for 48 h. The average for all three PMOXA-*g*(SS)-PCL **1** – **3** is given, due to non-significant differences between the samples. All the data are presented as the average ± SEM (n ≥ 3). Statistics were analyzed using two-tailed Student's *t*-test: $^{*}P<0.05$, $^{**}P<0.01$, $^{***}P<0.001$.

Graft copolymer biocompatibility and drug delivery studies with cancer cells

Primary evaluation of our reduction-sensitive nanoparticle platform for the smart delivery of drugs was performed on an *in vitro* cancer cell model (Fig. 4). First, cellular toxicity of the synthesized graft copolymers was tested on HeLa cells using cell-viability assays. These assays demonstrated that the three PMOXA-*g*(SS)-PCL copolymers were not toxic to HeLa cells in the concentration range of 0.1 mg/mL up to 1 mg/mL after 48 h incubation (Fig. 4D). This confirms biocompatibility of this new copolymer at the cellular level confirming its potential as a valuable candidate for smart drug delivery research and applications. Next, drug-loaded (DOX) nanoparticles were tested on HeLa cells to validate triggered drug delivery to cancer cells (Fig. 4, S16, S17, S18).

Confocal laser scanning microscopy (CLSM) was used to investigate cellular uptake and intracellular release behavior of DOX-loaded PMOXA-*g*(SS)-PCL nanoparticles in HeLa cells over the time course of 8 h (Fig. 4B, S16A, S17A, S18A). DOX intercalates with cellular DNA when released in cells causing a co-localization of fluorescence signals of DOX and the DNA-stain.[60] CLSM images demonstrate that DOX has been released from DOX-loaded PMOXA-*g*(SS)-PCL **2** nanoparticles (0.25 µg/mL DOX) and it has been transferred to the cell nucleus within only one hour (Fig. 4B). This indicates fast internalization of DOX-loaded nanoparticles and rapid release of DOX inside cells. These findings are comparable with free DOX (0.25 µg/mL DOX), which also mainly accumulated in the cell nucleus after 1 h (Fig. 4C). The fast release was attributed to the disulfide bond cleavage in the presence of high concentration of GSH (2–10 mM) in the intracellular compartment of cancer cells,[29] as demonstrated in the previous sections by extracellular NMR, DLS, TEM, and FCS measurements in 10 mM DTT and 10 mM GSH in case of FCS. The faster intracellular release of DOX compared to the extracellular FCS measurements with 10 mM GSH (Fig. S14D) are explained by the much more complex intracellular environment as explained above.[59]

DOX-loaded, reduction-sensitive PMOXA-*g*(SS)-PCL nanoparticles exhibited a higher anti-proliferation effect on HeLa cells compared to the non-sensitive DOX-loaded PMOXA-*b*-PCL nanoparticles at concentrations that led to significant reduction of cell viability in case of nanoparticles after 48 h incubation (4.5 and 9 µg/mL DOX, Fig. 4E). This was attributed to the fast, triggered, and efficient release form PMOXA-*g*(SS)-PCL nanoparticles compared to a slower, less efficient release from non-triggered, biodegradable nanoparticles formed from PMOXA-*b*-PCL. This explains the benefit of the reducible group in PMOXA-*g*(SS)-PCL compared to the non-sensitive linkage in PMOXA-*b*-PCL. PMOXA-*b*-PCL serves as a control to estimate the release from nanoparticles built from PMOXA and PCL in the absence of a responsive group. There was no difference observed between the three different PMOXA-*g*(SS)-PCL nanoparticles, which is why averages including all samples are given. Free DOX exhibited higher cytotoxicity at most of the concentrations, only at the highest concentration (9 µg/mL) there was no significant difference found to DOX delivered via reduction-sensitive nanoparticles. The cytotoxicity of DOX-loaded PMOXA-*g*(SS)-PCL nanoparticles is clearly related to the action of released DOX due to the non-toxic nature of PMOXA-*g*(SS)-PCLs up to 1 mg/mL (Fig. 4D); maximum concentration of polymer used within the DOX cytotoxicity assays was 0.07 mg/mL. The reduction-responsive nanoparticles efficiently deliver DOX to cancer cells to reach the full potential of the drug (Fig. 4E) while protecting it in the surrounding medium (Fig. 3C, S15). This will allow reducing the toxic side effects of DOX by keeping the drug within the stable nanoparticles after intravenous application – restricting vast distribution of the drug – followed by passive accumulation within tumor tissue, uptake by cancer cells and subsequent efficient intracellular release of the drug.

Drug delivery to *Plasmodium falciparum*-infected red blood cells

Another disease model was used to study the broad applicability of the reduction-sensitive PMOXA-*g*(SS)-PCL nanoparticle platform for smart drug delivery. Several pathways for the efficient nanoparticle uptake by parasitized RBCs, which can be utilized to passively target drug-loaded nanostructures to iRBCs compared to RBCs,[36,41,42] have been proposed.[43] However, it is still not clear which or which combination of these mechanisms allow targeted antimalarial delivery to iRBCs. Nevertheless, we make use of this iRBC "leakiness" to deliver loaded nanoparticles specifically to iRBCs compared to RBCs.

First, a model hydrophobic molecule, NileRed, was encapsulated in reduction-sensitive PMOXA-*g*(SS)-PCL **3** nanoparticles and PMOXA-*b*-PCL nanoparticles to study delivery of a model compound via fluorescence microscopy. This hydrophobic dye molecule additionally serves as a model for drug molecules with very low aqueous solubility, a property of many experimental drugs at early stages of drug development. After a short 2 h incubation of either free dye or encapsulated dye with a mixture of RBCs and iRBCs (about 4%), a clear intracellular parasite staining was observed in all cases, demonstrating the possible passively targeted delivery of a model molecule to iRBCs using small nanoparticles (Fig. 5B, S19). The dye is preferentially found in iRBCs compared to normal RBCs, which demonstrates a passive targeting. Further increase of iRBC targeting might be achieved by including additional targeting ligands (*e.g.* antibodies) on the nanostructure.[61] Since the passive targeting to iRBCs is already pronounced for non-targeted nanostructures,[61] as also shown herein, it allows to design less expensive drug carriers. The fast delivery of a model compound to iRBCs without any targeting ligands on the nanoparticle surface indicates the potential of inert, protein-repellant PMOXA-coated nanoparticles for passively targeted antimalarial delivery to *Plasmodium*-infected RBCs.

Fluorescence intensities were in general higher within schizonts compared to trophozoite stage parasites (Fig. S19).

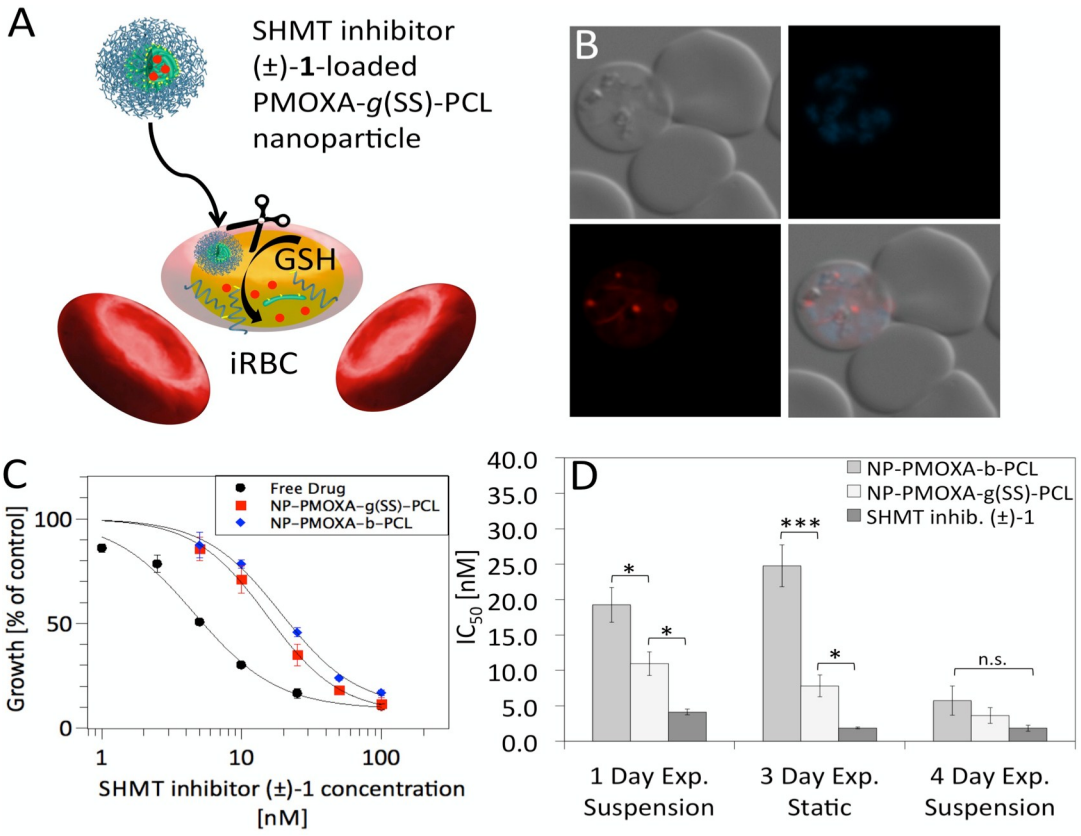

Fig. 5 Dye and drug delivery to *Plasmodium*-infected red blood cells (iRBCs). (A) Schematic representation of SHMT inhibitor (±)-**1** delivery to iRBCs using reduction-responsive PMOXA-*g*(SS)-PCL nanoparticles. (B) Fluorescence imaging demonstrating delivery of hydrophobic model molecule, NileRed, using PMOXA-*g*(SS)-PCL **3** nanoparticles: DIC (top left), Hoechst DNA-stain (top right), NileRed signal (bottom left), merge (bottom right). (C) Example of dose-response curves for one-day suspension antimalarial assay with free SHMT inhibitor (±)-**1** or nanoparticle-based delivery. (D) Comparison of IC_{50} values for all the different antimalarial assay conditions and samples presented as the average ± SEM (n ≥ 3). Statistics were analyzed using two-tailed Student's *t*-test: $^{*}P<0.05$, $^{**}P<0.01$, $^{***}P<0.001$.

The staining pattern shows accumulation of the dye in certain parasite compartments. This specific dye is known to accumulate in neutral lipid bodies, which were proposed to be storage organelles for lipid intermediates.[62] This staining pattern is also common in other cell types such as yeast cells.[63] The observation of this lipid body staining also in nanoparticle samples suggests successful release of the dye from nanoparticles. Combined with the high medium stability of both particles for several days (Fig. 3C, S15) it can be speculated that nanoparticles are taken up and the dye is subsequently released. This delivery mechanism was also proposed by other research groups.[36,41,42] To reflect the potency of nanoparticle-based stabilization and delivery of small compounds, a one-day-old NileRed aqueous solution was additionally tested in the same way and compared to a fresh NileRed solution. It clearly showed that this model hydrophobic compound was not stable enough in solution for one day; it did not readily appear in the iRBCs compared to fresh dye (Fig. S20).

Similarly, an experimental antimalarial compound (SHMT inhibitor (±)-**1**, Scheme 1),[32] which is very active *in vitro*, but with an intrinsic solubility and metabolic stability problem that hampers successful *in vivo* application,[32] was incorporated within reduction-sensitive and non-sensitive nanoparticles. With our nanoparticles, we could stabilize the drug up to concentrations of about 300 µM, whereas the free drug was not readily soluble in PBS, it visibly precipitated as shown in digital images at a concentration of 10 µM drug in PBS (Fig. S21). iRBCs and uninfected RBCs under shaking conditions were used as an *in vitro* system that more closely simulates the *in vivo* situation compared to standard static drug testing for antimalarials,[64] which was additionally performed (Fig. 5C,D). Only PMOXA-*g*(SS)-PCL **3** and PMOXA-*b*-PCL nanoparticles were used for antimalarial testing, because there were no significant differences found for the three graft copolymers in terms of drug delivery to cancer cells (Fig. 4). Solubilization and potential protection from metabolic degradation are the main reasons for SHMT inhibitor (±)-**1** encapsulation in nanoparticles.

We demonstrated that over two parasite cycles (four day suspension assay, 5% hematocrit) the drug reached its full potential when delivered via nanoparticles (Fig. 5D). For shorter incubation times (one day suspension assay, 10% hematocrit, Fig. 5C,D), the drug was more active followed by drug delivery via reduction-sensitive nanoparticles and non-sensitive nanoparticles. The results were similar when tested

in standard antimalarial drug testing assays (three day static assay, 1.25% hematocrit). In these *in vitro* settings, where no other cells apart from RBCs and iRBCs were present, developed antimalarials intrinsically target the iRBCs and uptake of bigger nanoparticles is slower compared to small molecule uptake. However, nanoparticles (< 80 nm diameter)[36,41,42] also passively target iRBCs compared to RBCs. This explains the delivery profile obtained with our drug delivery system, which indicates a somewhat delayed delivery of the antimalarial when delivered to iRBCs using nanoparticles. The mechanism of uptake has to be studied in more detail in the future. Nevertheless, the delivery profile obtained with our nanoparticle platform can be advantageous as demonstrated for artemisinin-loaded liposomes.[65,66] The liposomal formulation of artemisinin allowed to achieve a more stable drug concentration in the bloodstream and immediate effect on the parasites compared to free drug that was rapidly eliminated from the blood and only had an effect on the parasites several days after treatment start.[65,66] Compared to artemisinin, the SHMT inhibitor (±)-**1** used herein is not active at all against malaria *in vivo*.[32] Therefore, slightly higher *in vitro* activity of the free drug compared to nanoparticle-stabilized drug has to be seen from another angle. The nanoparticles solubilize and can further protect the drug from fast degradation, which will overcompensate the slightly slower uptake and activity of nanoparticle-based delivery. The chemical nature of the PMOXA-based nanoparticles provides the basis for prolonged circulation times in the blood,[15,17,18] and the hydrophobic core shields the drug from the environment before entering iRBCs; this is not possible with free SHMT inhibitor (±)-**1**.[32] An additional benefit of reduction-triggered delivery of antimalarials via nanoparticles would be the faster and more efficient drug release within even more reducing cytosols of drug-resistant parasites compared to drug-sensitive strains.[45,46]

Our nanoparticle platform holds the promise to efficiently solubilize and delay fast liver degradation of experimental antimalarial drug candidates, in order to reach a more stable drug blood drug concentration compared to free drug administration. These observations provide the basis for further optimization and application of nanoparticles for stabilizing, protecting, and delivering water-insoluble, labile drugs already at early stages of drug development. This represents a highly promising alternative to optimization of the drug itself and can be applied to other anticancer and anti-infectious drugs.

Conclusions

A library of reduction responsive PMOXA-*g*(SS)-PCL amphiphilic block copolymers was synthesized through the thiol-disulfide exchange reaction between thiolated PMOXA (PMOXA-SH) and pyridyl disulfide functionalized poly(ε-caprolactone) (PCL-*co*-PPCL). This type of copolymers self-assembled into nanoparticles with sizes around 50 nm. These nanoparticles did not reveal any cytotoxicity in the tested concentration range, providing a biocompatible, biodegradable, and reduction-triggerable platform for smart drug delivery. Detailed stability and release studies using nanoparticle-incorporated model compounds demonstrated high colloidal stability and guest molecule retention within the nanostructures when incubated in various cell media at physiological temperature for four days. Rapid release of the guest molecules was achieved upon treatment with biologically relevant reducing agent concentrations. This designed nanoparticle platform was successfully used to deliver hydrophobic, toxic anticancer drugs to cancer cells. Additionally, this nanoparticle platform was evaluated to solubilize and deliver a hydrophobic, metabolically unstable, experimental antimalarial drug to *Plasmodium*-infected RBCs, which was successfully achieved. Our new reduction-sensitive amphiphilic copolymers are promising candidate materials for targeted drug delivery purposes to tackle cancer and malaria with a sophisticated smart delivery platform.

Acknowledgements

This work was supported by the Swiss National Science Foundation, NCCR Molecular Systems Engineering, and the University of Basel and this is gratefully acknowledged. DW wishes to thank the China Scholarship Council for supporting the fee to study abroad.

Notes and references

‡ Equal contribution.

1 M. W. Tibbitt, J. E. Dahlman and R. Langer, *J. Am. Chem. Soc.*, 2016, **138**, 704–717.
2 V. P. Torchilin, *Adv. Drug Deliver. Rev.*, 2012, **64**, 302–315.
3 C. J. Cheng, G. T. Tietjen and J. K. Saucier-Sawyer, *Nat. Rev. Drug Discov.*, 2015, **14**, 239–247.
4 Y. Matsumura and H. Maeda, *Cancer Res.*, 1986, **46**, 6387–6392.
5 J. Fang, H. Nakamura and H. Maeda, *Adv. Drug Deliver. Rev.*, 2011, **63**, 136–151.
6 R. A. Petros and J. M. DeSimone, *Nat. Rev. Drug Discov.*, 2010, **9**, 615–627.
7 H. Cabral, J. Makino, Y. Matsumoto, P. Mi, H. Wu, T. Nomoto, K. Toh, N. Yamada, Y. Higuchi, S. Konishi, M. R. Kano, H. Nishihara, Y. Miura, N. Nishiyama and K. Kataoka, *ACS Nano*, 2015, **9**, 4957–4967.
8 A. Blanazs, S. P. Armes and A. J. Ryan, *Macromol. Rapid Commun.*, 2009, **30**, 267–277.
9 D. Wu, M. Spulber, F. Itel, M. Chami, T. Pfohl, C. G. Palivan and W. Meier, *Macromolecules*, 2014, **47**, 5060–5069.
10 G. Gunkel-Grabole, S. Sigg, M. Lomora, S. Lörcher, C. G. Palivan and W. P. Meier, *Biomater. Sci.*, 2015, **3**, 25–40.
11 C. Oerlemans, W. Bult, M. Bos, G. Storm, J. F. W. Nijsen and W. E. Hennink, *Pharm. Res.*, 2010, **27**, 2569–2589.
12 C. G. Palivan, R. Goers, A. Najer, X. Zhang, A. Car and W. Meier, *Chem. Soc. Rev.*, 2016, **45**, 377–411.
13 J. Nicolas, S. Mura, D. Brambilla, N. Mackiewicz and P. Couvreur, *Chem. Soc. Rev.*, 2013, **42**, 1147–1235.
14 S. Zhang, J. Zou, M. Elsabahy, A. Karwa, A. Li, D. A. Moore, R. B. Dorshow and K. L. Wooley, *Chem. Sci.*, 2013, **4**, 2122.

15 K. Knop, R. Hoogenboom, D. Fischer and U. S. Schubert, *Angew. Chem. Int. Ed.*, 2010, **49**, 6288–6308.
16 W. Jiskoot, R. M. F. Schie, M. G. Carstens and H. Schellekens, *Pharm. Res.*, 2009, **26**, 1303–1314.
17 R. Hoogenboom, *Angew. Chem. Int. Ed.*, 2009, **48**, 7978–7994.
18 M. Barz, R. Luxenhofer, R. Zentel and M. J. Vicent, *Polym. Chem.*, 2011, **2**, 1900–1918.
19 S. Mura, J. Nicolas and P. Couvreur, *Nat. Mater.*, 2013, **12**, 991–1003.
20 Y. Lu, W. Sun and Z. Gu, *J. Control. Release*, 2014, **194**, 1–19.
21 V. P. Torchilin, *Nat. Rev. Drug Discov.*, 2014, **13**, 813–827.
22 H. J. Kim, K. Miyata, T. Nomoto, M. Zheng, A. Kim, X. Liu, H. Cabral, R. J. Christie, N. Nishiyama and K. Kataoka, *Biomaterials*, 2014, **35**, 4548–4556.
23 Y. Li, T. Liu, G. Zhang, Z. Ge and S. Liu, *Macromol. Rapid Commun.*, 2014, **35**, 466–473.
24 S. Yu, J. Ding, C. He, Y. Cao, W. Xu and X. Chen, *Adv. Healthcare Mater.*, 2013, **3**, 752–760.
25 M. Huo, J. Yuan, L. Tao and Y. Wei, *Polym. Chem.*, 2014, **5**, 1519–1528.
26 T. Thambi, V. G. Deepagan, H. Ko, Y. D. Suh, G.-R. Yi, J. Y. Lee, D. S. Lee and J. H. Park, *Polym. Chem.*, 2014, **5**, 4627–4634.
27 Q. Zhang, S. Aleksanian, S. M. Noh and J. K. Oh, *Polym. Chem.*, 2013, **4**, 351–359.
28 R. Cheng, F. Feng, F. Meng, C. Deng, J. Feijen and Z. Zhong, *J. Control. Release*, 2011, **152**, 2–12.
29 F. Q. Schafer and G. R. Buettner, *Free Radic. Biol. Med.*, 2001, **30**, 1191–1212.
30 M. Narvekar, H. Y. Xue, J. Y. Eoh and H. L. Wong, *AAPS PharmSciTech*, 2014, **15**, 822–833.
31 M. Witschel, M. Rottmann, M. Kaiser and R. Brun, *PLoS Negl. Trop. Dis.*, 2012, **6**, e1805.
32 M. C. Witschel, M. Rottmann, A. Schwab, U. Leartsakulpanich, P. Chitnumsub, M. Seet, S. Tonazzi, G. Schwertz, F. Stelzer, T. Mietzner, C. McNamara, F. Thater, C. Freymond, A. Jaruwat, C. Pinthong, P. Riangrungroj, M. Oufir, M. Hamburger, P. Mäser, L. M. Sanz-Alonso, S. Charman, S. Wittlin, Y. Yuthavong, P. Chaiyen and F. Diederich, *J. Med. Chem.*, 2015, **58**, 3117–3130.
33 A. F. Cowman, D. Berry and J. Baum, *J. Cell Biol.*, 2012, **198**, 961–971.
34 K. M. Tun, M. Imwong, K. M. Lwin, A. A. Win, T. M. Hlaing, T. Hlaing, K. Lin, M. P. Kyaw, K. Plewes, M. A. Faiz, M. Dhorda, P. Y. Cheah, S. Pukrittayakamee, E. A. Ashley, T. J. C. Anderson, S. Nair, M. McDew-White, J. A. Flegg, E. P. M. Grist, P. Guerin, R. J. Maude, F. Smithuis, A. M. Dondorp, N. P. J. Day, F. Nosten, N. J. White and C. J. Woodrow, *Lancet Infect. Dis.*, 2015, **15**, 415–421.
35 C. Amaratunga, P. Lim, S. Suon, S. Sreng and S. Mao, *Lancet Infect. Dis.*, 2016, **16**, 357–365.
36 P. Urbán, J. J. Valle-Delgado, N. Mauro, J. Marques, A. Manfredi, M. Rottmann, E. Ranucci, P. Ferruti and X. Fernàndez-Busquets, *J. Control. Release*, 2014, **177**, 84–95.
37 J. Movellan, P. Urbán, E. Moles, J. M. de la Fuente, T. Sierra, J. L. Serrano and X. Fernàndez-Busquets, *Biomaterials*, 2014, **35**, 7940–7950.
38 N. S. Santos-Magalhães and V. C. F. Mosqueira, *Adv. Drug Deliver. Rev.*, 2010, **62**, 560–575.
39 E. Dennis, V. A. Peoples and F. Johnson, *J. Infect. Dis. Ther.*, 2015, **3**, 1–6.
40 E. S. Bergmann-Leitner, E. H. Duncan and E. Angov, *Malar. J.*, 2009, **8**, 183–195.
41 I. D. Goodyer, B. Pouvelle, T. G. Schneider, D. P. Trelka and T. F. Taraschi, *Mol. Biochem. Parasitol.*, 1997, **87**, 13–28.
42 A. El Tahir, P. Malhotra and V. S. Chauhan, *Malar. J.*, 2003, **2**, 1–8.
43 K. Kirk, *Physiol. Rev.*, 2001, **81**, 495–537.
44 D. Kasozi, F. Mohring, S. Rahlfs, A. J. Meyer and K. Becker, *PLoS Pathog.*, 2013, **9**, e1003782.
45 V. L. Dubois, D. F. Platel, G. Pauly and J. Tribouley-Duret, *Exp. Parasitol.*, 1995, **81**, 117–124.
46 J. Vega-Rodríguez, R. Pastrana-Mena, K. N. Crespo-Lladó, J. G. Ortiz, I. Ferrer-Rodríguez and A. E. Serrano, *PLoS ONE*, 2015, **10**, e0128212.
47 C. Nardin, T. Hirt, J. Leukel and W. Meier, *Langmuir*, 2000, **16**, 1035–1041.
48 B. Pidhatika, M. Rodenstein, Y. Chen, E. Rakhmatullina, A. Mühlebach, C. Acikgöz, M. Textor and R. Konradi, *Biointerphases*, 2012, **7**, 1–15.
49 S. Zalipsky, C. B. Hansen, J. M. Oaks and T. M. Allen, *J. Pharm. Sci.*, 1996, **85**, 133–137.
50 A. Mahmud, X.-B. Xiong and A. Lavasanifar, *Macromolecules*, 2006, **39**, 9419–9428.
51 W. Chen, Y. Zou, J. Jia, F. Meng, R. Cheng, C. Deng, J. Feijen and Z. Zhong, *Macromolecules*, 2013, **46**, 699–707.
52 G.-H. Hsiue, H.-Z. Chiang, C.-H. Wang and T.-M. Juang, *Bioconjugate Chem.*, 2006, **17**, 781–786.
53 C. Cui, Y.-N. Xue, M. Wu, Y. Zhang, P. Yu, L. Liu, R.-X. Zhuo and S.-W. Huang, *Biomaterials*, 2013, **34**, 3858–3869.
54 H. Sun, F. Meng, R. Cheng, C. Deng and Z. Zhong, *Expert Opin. Drug Deliv.*, 2013, **10**, 1109–1122.
55 T. Yamaoka, Y. Tabata and Y. Ikada, *J. Pharm. Sci.*, 1994, **83**, 601–606.
56 P. Rigler and W. Meier, *J. Am. Chem. Soc.*, 2006, **128**, 367–373.
57 S. Toughraï, V. Malinova, R. Masciadri, S. Menon, P. Tanner, C. Palivan, N. Bruns and W. Meier, *Macromol. Biosci.*, 2015, **15**, 481–489.
58 P. A. Johnston, *Curr. Opin. Chem. Biol.*, 2011, **15**, 174–182.
59 D. Yu, G. Zou, X. Cui, Z. Mao, I. Estrela-Lopis, E. Donath and C. Gao, *J. Mater. Chem. B*, 2015, **3**, 8865–8873.
60 O. Tacar, P. Sriamornsak and C. R. Dass, *J. Pharm. Pharmacol.*, 2012, **65**, 157–170.
61 P. Urbán, J. Estelrich, A. Cortés and X. Fernàndez-Busquets, *J. Control. Release*, 2011, **151**, 202–211.
62 K. E. Jackson, N. Klonis, D. J. P. Ferguson, A. Adisa, C. Dogovski and L. Tilley, *Mol. Microbiol.*, 2004, **54**, 109–122.
63 F. Ciamponi, C. Duckham and N. Tirelli, *Appl. Microbiol. Biotechnol.*, 2012, **95**, 1445–1456.
64 A. Najer, D. Wu, A. Bieri, F. Brand, C. G. Palivan, H.-P. Beck and W. Meier, *ACS Nano*, 2014, **8**, 12560–12571.
65 B. Isacchi, S. Arrigucci, G. L. Marca, M. C. Bergonzi, M. G. Vannucchi, A. Novelli and A. R. Bilia, *J. Lipos. Res.*, 2011, **21**, 237–244.
66 B. Isacchi, M. C. Bergonzi, M. Grazioso, C. Righeschi, A. Pietretti, C. Severini and A. R. Bilia, *Eur. J. Pharm. Biopharm.*, 2012, **80**, 528–534.